AJNR

Application of Time-Resolved 3D Digital Subtraction Angiography to Plan Cerebral Arteriovenous Malformation Radiosurgery

K.-K. Chen, W.-Y. Guo, H.-C. Yang, C.-J. Lin, C.-H.F. Wu, S. Gehrisch, M. Kowarschik, Y.-T. Wu and W.-Y. Chung

AJNR Am J Neuroradiol published online 26 January 2017
http://www.ajnr.org/content/early/2017/01/26/ajnr.A5074

Published January 26, 2017 as 10.3174/ajnr.A5074

Application of Time-Resolved 3D Digital Subtraction Angiography to Plan Cerebral Arteriovenous Malformation Radiosurgery

K.-K. Chen, W.-Y. Guo, H.-C. Yang, C.-J. Lin, C.-H.F. Wu, S. Gehrisch, M. Kowarschik, Y.-T. Wu, and W.-Y. Chung

ABSTRACT

BACKGROUND AND PURPOSE: Time-resolved 3D-DSA (4D-DSA) enables viewing vasculature from any desired angle and time frame. We investigated whether these advantages may facilitate treatment planning and the feasibility of using 4D-DSA as a single imaging technique in AVM/dural arteriovenous fistula radiosurgery.

MATERIALS AND METHODS: Twenty consecutive patients (8 dural arteriovenous fistulas and 12 AVMs; 13 men and 7 women; mean age, 45 years; range, 18–64 years) who were scheduled for gamma knife radiosurgery were recruited (November 2014 to October 2015). An optimal volume of reconstructed time-resolved 3D volumes that defines the AVM nidus/dural arteriovenous fistula was sliced into 2D-CT-like images. The original radiosurgery treatment plan was overlaid retrospectively. The registration errors of stereotactic 4D-DSA were compared with those of integrated stereotactic imaging. AVM/dural arteriovenous fistula volumes were contoured, and disjoint and conjoint components were identified. The Wilcoxon signed rank test and the Wilcoxon rank sum test were adopted to evaluate registration errors and contoured volumes of stereotactic 4D-DSA and integration of stereotactic MR imaging and stereotactic 2D-DSA.

RESULTS: Sixteen of 20 patients were successfully registered in Advanced Leksell GammaPlan Program. The registration error of stereotactic 4D-DSA was smaller than that of integrated stereotactic imaging ($P = .0009$). The contoured AVM volume of 4D-DSA was smaller than that contoured on the integration of MR imaging and 2D-DSA, while major inconsistencies existed in cases of dural arteriovenous fistula ($P = .042$ and 0.039, respectively, for measurements conducted by 2 authors).

CONCLUSIONS: Implementation of stereotactic 4D-DSA data for gamma knife radiosurgery for brain AVM/dural arteriovenous fistula is feasible. The ability of 4D-DSA to demonstrate vascular morphology and hemodynamics in 4 dimensions potentially reduces the target volumes of irradiation in vascular radiosurgery.

ABBREVIATION: DAVF = dural arteriovenous fistula

Radiosurgery is an effective treatment alternative for cerebral arteriovenous malformations[1-4] and intracranial dural arteriovenous fistulas (DAVFs).[5-10] In AVM/DAVF radiosurgery, irradiation is delivered in a single fraction stereotactically to only the nidus of an AVM or fistula of a DAVF.

Our current clinical practice of AVM/DAVF radiosurgery, integrated stereotactic imaging (MR imaging/MRA and x-ray digital subtraction angiography) is used for nidus/fistula delineation. The integrated multiple-stop stereotactic imaging is considered the reference imaging for AVM/DAVF radiosurgery. MR imaging is superior in delineating radiosurgical target in 3D, and DSA excels in defining the hemodynamics of AVM/AVF and differentiating the nidus/fistula from feeding arteries and draining veins of AVM/DAVF.[11] However, the role of DSA as a projective 2D representation of 3D structures in defining the nidus is limited, especially when the AVM is large and the nidus has an oblique long axis relative to the orthogonal DSA projections.[12] Moreover, for AVMs that undergo partial embolization before radiosurgery, the nidus may become intricate, and it may be difficult to define its morphology on 2D-DSA or MR imaging/MRA.[13] Recently, it

Received September 27, 2016; accepted after revision November 18.

From the Department of Biomedical Imaging and Radiological Sciences (K.-K.C., Y.-T.W.), National Yang-Ming University, Taipei, Taiwan; Departments of Radiology (W.-Y.G., C.-J.L.) and Neurosurgery (H.-C.Y., W.-Y.C.), Taipei Veterans General Hospital, Taipei, Taiwan; School of Medicine (W.-Y.G., C.-J.L.), National Yang-Ming University, Taipei, Taiwan; Siemens Healthcare Ltd, Advanced Therapies (C.-H.F.W.), Taipei, Taiwan; and Siemens, Advanced Therapies (S.G., M.K.), Forchheim, Germany.

The experimental software presented in this article is based on research. Due to regulatory reasons, its future availability cannot be guaranteed.

The research was sponsored by Ministry of Science and Technology (103-2314-B-075-064 MY2). The materials are, in part, from collaboration between Taipei Veterans General Hospital, Taiwan, and Siemens.

Please address correspondence to Wan-Yuo Guo, MD, PhD, Department of Radiology, Taipei Veterans General Hospital, 201, Section II, Shih-Pai Rd, Taipei, Taiwan, TW 112; e-mail: wyguo@vghtpe.gov.tw; @KKChen0438

Indicates open access to non-subscribers at www.ajnr.org

http://dx.doi.org/10.3174/ajnr.A5074

was shown that conebeam CT 3D angiography can generate images of a high spatial resolution that depict low-flow nidal compartments better than both DSA and MR imaging, though it lacks temporal information.[14] While our current practice has achieved high tissue conformity in AVM radiosurgery and good therapeutic results,[15] an alternative technique, if chosen, must be able to provide panoramic morphological and hemodynamic evaluation of nidi/fistulas in 1 stop.

In contrast to 2D-DSA, fully time-resolved 3D-DSA, also known as 4D-DSA, provides a series of time-resolved 3D volumes that correspond to contrast dynamics with a C-arm-based imaging system.[16] While the reconstruction of a 4D-DSA image from a single rotational image acquisition has some inherited technical difficulties, as mentioned by Royalty,[17] the volumetric vascular morphology and bolus-arrival patterns reconstructed from 4D-DSA algorithms are validated.[17] An animal study based on a canine model also demonstrated that 4D-DSA is capable of delineating vasculature effectively.[18] Small-series studies also suggested that 4D-DSA enhances the ability to visualize the vascular anatomy of an AVM.[19,20] Accordingly, 4D-DSA enables evaluating feeding arteries, nidi, and draining veins in sequential imaging in 3D and eliminates the issue of overlapped vasculatures.

In this study, we compare the registration errors of stereotactic 4D-DSA with those of integrated stereotactic imaging and the vascular anatomy of AVMs and DAVFs depicted by 4D-DSA volumes with the planned dose contours for each recruited patient and evaluate whether 4D-DSA may facilitate the planning of AVM/DAVF radiosurgery by minimizing the irradiation volume as 1-stop imaging.

MATERIALS AND METHODS

This is a retrospective study for feasibility evaluation of implementing 4D-DSA in AVM/DAVF radiosurgery. Under the approval of the institutional review board of Taipei Veterans General Hospital, 20 consecutive patients (8 with DAVFs and 12 with AVMs; 13 men and 7 women; mean age, 45 years; range, 18–64 years; men, mean age of 48 years; range, 18–66 years; women, mean age of 47 years; range, 32–64 years) who underwent radiosurgery (November 2014 to October 2015) with gamma knife and treatment planning with the Advanced Leksell GammaPlan Program (Elekta, Stockholm, Sweden) were recruited.

The treatment plans of these radiosurgeries and the stereotactic imaging used for planning the treatments were retrieved to evaluate the potential role of time-resolved 3D-DSA in radiosurgery. Here, the stereotactic imaging included stereotactic MR imaging and stereotactic 2D-DSA with the routine protocols used for decades since the early stage of radiosurgery service.[5,7,10-12,15] Time-resolved 3D-DSA was included in the data acquisition to facilitate the target visual perception for planning radiosurgery. Both 2D and time-resolved 3D-DSA were performed by using a biplane angiography system (Artis zee; Siemens, Erlangen, Germany). A total volume of 24–41 mL of Omnipaque 300 (iohexol; GE Healthcare, Piscataway, New Jersey) contrast agent was injected at either the patient's internal carotid artery or common carotid artery. An imaging protocol that covers an angular range of 260° within an acquisition time of approximately 12 seconds

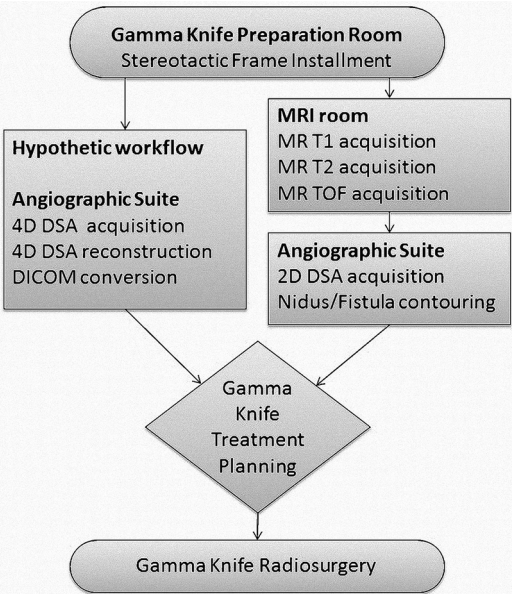

FIG 1. Hypothetic workflow of importing 4D-DSA into the treatment plan computer (Advanced Leksell GammaPlan Program; Elekta) and the workflow of the current practice. Application of the stereotactic frame to the patient's skull and measurement of skull geometry are performed first in the preparation room.

was used, generating 304 raw projections from consecutive imaging angles. X-ray delay was set to 0.5 seconds.

Figure 1 summarizes the workflow of both the radiosurgical procedures as routinely conducted (right route) and the herein discussed hypothetic implementation of time-resolved 3D DSA into the procedure (left route). The stereotactic frame and basal ring were applied to a patient's head with 4 screws. On the basis of the diagnostic images acquired before radiosurgery, the frame was applied so that the screws did not overlap the AVM nidus in the orthogonal 2D-DSA projections and to avoid metallic artifacts that may occur in the subsequent postprocessing images. Stereotactic MR imaging and stereotactic DSA were performed sequentially. Different localization boxes were applied on the basal ring of the stereotactic frame for different imaging acquisitions. The markers on the localization boxes served as references for image registration and treatment planning. Neuroradiologists contoured the AVM nidus/DAVF on 2D DSA. For the hypothetic treatment planning, the raw projections were transferred to a research workstation (syngo X-workplace VB21; Siemens) equipped with the 4D-DSA prototype software. The raw projections of 4D-DSA were reconstructed into 304 time-dependent volumes and were assessed by 2 experienced neuroradiologists to select the optimal phase that best illustrated the AVM nidus/DAVF.

In Fig 2, a single optimal phase of the nidus/fistula opacification is selected from the 4D dynamic volume for each patient. It was observed that 4D-DSA provides better 3D delineation of the nidus than 2D-DSA in terms of morphology, particularly for larger and intricate nidi, because the feeding artery, nidus/fistula, and draining vein may overlap in the 2D projections. Four patients (1 with a DAVF and 3 with AVMs) were retrospectively excluded from the current analysis due to incomplete coverage of markers on the localization box installed, which subsequently rendered these stereo-

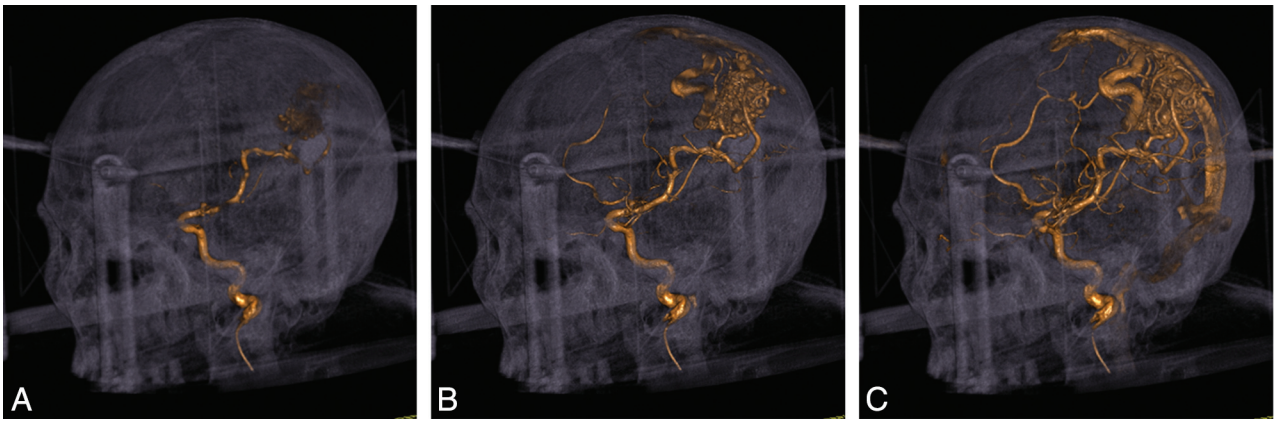

FIG 2. *A*, Early opacification phases of the AVM nidus, where only the feeding artery and a portion of the nidus are opacified. *B*, Middle opacification phases of the AVM nidus, in which both the feeding artery and nidus are opacified, as well as a portion of draining vein. This phase is optimal for nidus delineation. *C*, In the late opacification phase, the draining veins are completely opacified and may obstruct the visibility of the nidus.

Volume comparison of AVM nidus and DAVF fistula between 4D-DSA and integrated stereotactic imaging[a]

Diagnosis	4D-DSA Volume (1st/2nd) (cm^3)	MR Imaging Volume (cm^3)	Conjoint Volume (1st/2nd) (cm^3)	Disjoint Volume (1st/2nd) (cm^3)	Volume Shown by 4D-DSA Only (1st/2nd) (cm^3)	Volume Shown by MR Imaging Only (1st/2nd) (cm^3)
DAVF	14.51/11.4	13.16	8.07/7.55	11.52/9.46	6.44/3.85	5.08/5.61
DAVF	2.92/3.26	5.09	1.9/2.02	4.21/4.31	1.02/1.23	3.19/3.07
DAVF	3.13/2.38	1.63	0.81/0.82	3.14/2.37	2.31/1.56	0.82/0.81
DAVF	3.29/2.98	4.34	2.82/2.56	1.98/2.19	1.98/0.41	1.51/1.77
DAVF	2.1/1.94	3.57	1.71/1.65	2.23/2.19	0.38/0.28	1.85/1.91
DAVF	4.98/4.74	4.89	4.14/3.81	1.59/2	0.84/0.92	0.74/1.07
DAVF	1.84/1.94	1.83	1.24/1.16	1.18/1.44	0.6/0.78	0.58/0.66
AVM	5.82/6.1	9.52	5.78/6.02	3.78/3.57	0.04/0.07	3.73/3.5
AVM	0.1/0.09	0.12	0.07/0.06	0.07/0.08	0.02/0.03	0.04/0.05
AVM	12.19/12.2	14.87	11.63/11.6	3.8/3.87	0.56/0.6	3.24/3.27
AVM	3.56/3.79	3.56	2.46/2.55	2.19/2.25	1.09/1.24	1.09/1.01
AVM	0.15/0.16	0.18	0.11/0.12	0.1/0.1	0.03/0.06	0.06/0.04
AVM	4.2/3.99	5.01	3.54/3.43	2.12/2.13	0.66/0.56	1.46/1.57
AVM	3.93/3.86	5.86	3.83/3.67	2.12/2.37	0.09/0.18	2.02/2.19
AVM	3.61/3.31	3.42	3.18/2.95	0.68/0.83	0.43/0.36	0.24/0.47
AVM	1.18/1.16	1.3	1.02/1.01	0.43/0.45	0.15/0.15	0.27/0.29

[a] Target contouring on 4D-DSA was performed independently on Advanced Leksell GammaPlan Program by 2 physicians who were blinded to the MR images. In AVMs, the contoured volumes are smaller than those contoured on the basis of integrated stereotactic images. For DAVFs, the contouring on 4D-DSA was blocked; this outcome results in more prominent inconsistencies between volumes contoured on 4D-DSA and those of MR integrated stereotactic imaging.

tactic imaging volumes derived from 4D-DSA unable to be registered on the Advanced Leksell GammaPlan Program.

For every remaining patient, the selected optimal phase of the 4D volume was then sliced with 3-mm section thickness along the cranial-caudal direction without interspacing into 2D-CT-like images. The 2D-CT-like images were output in DICOM format and underwent header compatibility processing by using Matlab R2013b (MathWorks, Natick, Massachusetts). The 2D-CT-like DICOM images stemming from stereotactic 4D-DSA were then imported to GammaPlan for "hypothetic" treatment planning. Registration between the 2D-CT-like images and the digital phantom of the localization box was performed. The original treatment plans were retrieved and overlaid on these successfully imported images to evaluate the radiation coverage of the nidus/fistula depicted by 4D-DSA.

The current practice of treatment planning for AVM/DAVF radiosurgery in Taipei Veteran General Hospital encompasses multiple MR imaging series, including stereotactic T1-weighted, T2-weighted MR imaging, time-of-flight MRA, and stereotactic 2D-DSA. These images were registered onto the built-in digital model of GammaPlan, and registration errors were computed.

Contouring of the AVM nidus/DAVF on registered 2D-CT-like images was performed independently by 2 authors who were blinded to the stereotactic MR images. The contoured volumes of both 4D-DSA and integrated stereotactic imaging were exported to Matlab R2013b (MathWorks), and volume analysis was performed.[21,22] Conjoint and disjoint volumes between 4D-DSA and integrated stereotactic imaging were measured. The results are summarized in the Table.

The Wilcoxon signed rank test and the Wilcoxon rank sum test were used to evaluate registration errors and contoured volumes of stereotactic 4D-DSA and that of the integrated stereotactic imaging. A *P* value of .05 was used to determine the significance of the test.

RESULTS

Among 20 initially selected patients, 16 (80%) entered the final analysis of stereotactic registration for planning of radiosurgery.

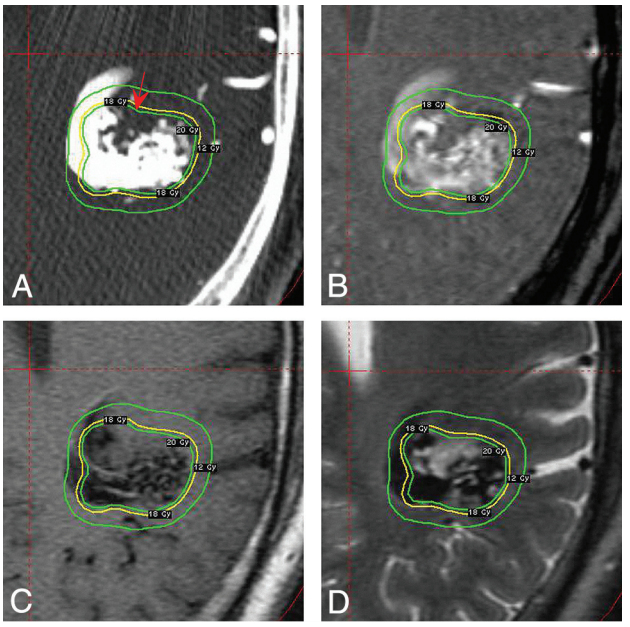

FIG 3. *A*, 4D-DSA of a 53-year-old man with a larger and more intricate AVM. The *red arrow* indicates a non-nidus territory, where it is considered part of AVM nidus based on the integrated MR images, enclosed within the irradiated volume. *B*, The corresponding TOF-MR imaging section. *C*, The T1-weighted MR image is shown on the same axial location. The nidus territory depicted by T1-weighted imaging is blurred. *D*, The T2-weighted MR image is shown on the same axial location. The T2-weighted MR imaging section provides clearer depiction of the nidus territory than the T1-weighted MR imaging because it does not show a flow void in the region in question.

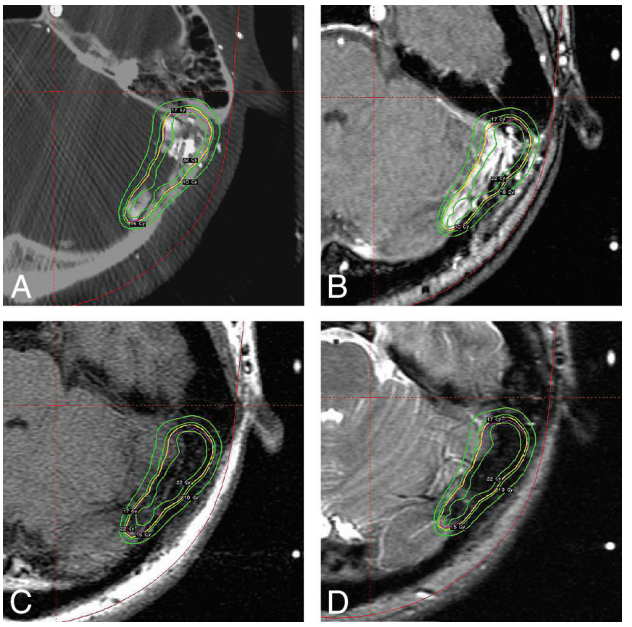

FIG 4. *A*, A 4D-DSA section of a 41-year-old man with a left sigmoid DAVF. The 4D-DSA provides opacification of the fistula. However, the central portion is empty. This feature may be attributed to technical difficulties or improper selection of an optimal frame. *B*, TOF-MR imaging of the same patient. TOF-MR imaging shows clear opacification of the fistula. *C*, The T1-weighted MR imaging section. The fistula is completely invisible; thus, the T1-weighted MR imaging is incapable of defining the fistula. *D*, T2-weighted MR imaging section. Defining the fistula is not feasible due to its invisibility on T2-weighted MR imaging as well.

In the other 20%, the "N" markers on the sides of the localization box were not completely covered in the FOV of 4D-DSA and failed in image registration.

The mean and standard error of stereotactic 4D-DSA for planning AVM/DAVF radiosurgery with Advanced Leksell GammaPlan Program of the 16 patients were 0.5588 ± 0.0631 mm. The corresponding mean and standard error of integrated stereotactic imaging registration of the patients were 1.0744 ± 0.0223 mm ($P = .0009$).

A patient with a large AVM is shown in Fig 3. The treatment plan is displayed as 3 isodose shells that correspond to dosages equivalent to 20 Gy, 18 Gy, and 12 Gy, from inside to outside the nidus. On the lower portion of the AVM, a region of normal brain tissue is enclosed within the planned dose coverage, as indicated in Fig 3*A*. In the original dose plan in which the delineation of the nidus was done by integrating multiple MR imaging series, including stereotactic TOF-MRA, T1-weighted MR imaging, T2-weighted MR imaging (Fig 3*B*, *-C*, and *-D*), and stereotactic 2D-DSA, the complexities of the hemodynamics of the AVM led to a portion of normal brain tissue being judged as part of the nidus on MR images, and it received therapeutic irradiation dose during the treatment.

A patient with a DAVF is shown in Fig 4. The fistula of the transverse sinus is large and complicated and runs obliquely. Both 4D-DSA (Fig 4*A*) and stereotactic TOF-MRA (Fig 4*B*) provide opacification of the fistula, while the fistula is less conspicuously seen on T1-weighted and T2-weighted MR imaging, as shown in Fig 4*C*, *-D*. However, the central portion of the fistula seems absent on 4D-DSA; this feature may be attributed to difficulty in the global thresholding of 4D-DSA or improper selection of an optimal phase for DAVF delineation. A proper hemodynamic phase selection from 304 frames of the full 4D series DSA and window setting may be essential for determining the extent of the segment of the sinus that contains fistulas.

The means and standard errors of the volumes of contoured AVMs and DAVFs on 4D-DSA were 3.86 ± 0.84 cm^3 and 4.39 ± 0.89 cm^3, respectively; and those of volumes of AVMs and DAVFs on integrated stereotactic imaging were 4.87 ± 1.59 cm^3 and 4.93 ± 2.01 cm^3. The mean and standard error of target volumes of all patients on 4D-DSA were 4.09 ± 0.64 cm^3, and those of integrated stereotactic imaging were 4.9 ± 1.06 cm^3. The contoured volumes on 4D-DSA and integrated stereotactic imaging were taken as pair samples, and the Wilcoxon signed rank test was performed. For volumes measured by the first measurement, the *P* values of the test performed on patients with DAVFs, AVMs, and all patients were .937, .039, and .098, respectively; and those of the second measurement were .109, .039, and .011, respectively.

It was observed that the inconsistencies between contoured 4D-DSA and integrated stereotactic imaging volumes of DAVFs were larger than those of patients with AVMs, as shown in Fig 5. To identify these inconsistencies, the patients with DAVFs and AVMs were taken as distinct groups, and the disjoint volumes between 4D-DSA and integrated stereotactic imaging were converted to percentages. The Wilcoxon rank sum test was applied, and the *P* values of the test for the first and second measurements were .042 and .031.

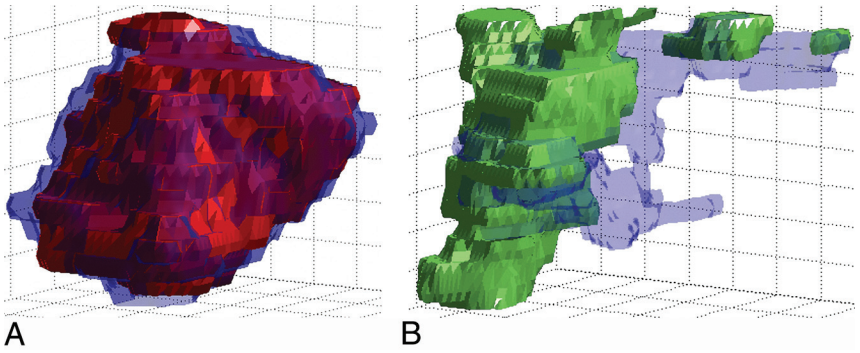

FIG 5. *A*, 3D rendering of contoured AVM volumes in Matlab. The *semitransparent blue shell* is the volume contoured by using integrated stereotactic imaging, whereas the *solid red mesh* depicts the volume contoured on 4D-DSA. Generally, the contoured volume of 4D-DSA is visually consistent with that of integrated stereotactic imaging. *B*, 3D rendering of contoured DAVF volumes in Matlab. The *semitransparent blue shell* is the volume contoured with integrated stereotactic imaging, whereas the solid *green mesh depicts* the volume contoured on 4D-DSA. Inconsistency between the 2 volumes is obvious.

DISCUSSION

This study investigates the ability of 4D-DSA to define the morphology of the nidus/fistula of AVM/DAVF in radiosurgery by porting the 4D-DSA images into Advanced Leksell GammaPlan Program and retrospectively overlaying the treatment plan. Contoured target volumes were statistically compared between 4D-DSA and integrated stereotactic imaging.

The current practice of radiosurgery, which involves integrated stereotactic 2D-DSA and stereotactic MR imaging, has achieved a high cure rate, particularly for small AVMs and residual AVMs after partial elimination in radiosurgery.[12] Other small-series studies also used combined imaging, including 3D rotational angiography, for radiosurgery treatment planning.[14,23,24] However, the hemodynamics and temporal information inherent in 3D rotational angiography are limited.

Although the integrated stereotactic 2D-DSA and stereotactic MR imaging are adopted as the reference imaging guidance for radiosurgery, conventional MR imaging techniques are suboptimal for evaluating the hemodynamics of AVMs. Conventional MR imaging techniques also have limited sensitivity for small AVM nidi.[25] Despite that the advancements in MR imaging technique such as 4D-MRA have enabled temporal information to be recorded, its limitations are still prominent.[26,27] Additionally, differences in AVM nidus contouring–derived MR images increase the likelihood of mismatch between the dose contour and the exact nidus volume during treatment planning.

Stereotactic 4D-DSA may facilitate the treatment planning by providing the hemodynamics and morphology of AVM/DAVF in 1 stop. The 4D-DSA has been shown to provide higher temporal and spatial resolution than current MR imaging/MRA and CT angiography.[16] In addition, 4D reconstructions allow examining the vasculature from any angle with any desired temporal point, which can facilitate the delineation of a nidus by judging the sequential appearance of different components of feeding arteries, nidi/fistulas, and draining veins of AVMs or DAVFs.

At the current stage, we used 4D-DSA as a supplementary technique to investigate whether it can be integrated into the treatment planning of gamma knife radiosurgery. Our approach was to retrospectively and hypothetically apply 2D-CT-like images from stereotactic 4D-DSA volumes to radiosurgery treatment planning that is currently based on integrated stereotactic 2D DSA and MR imaging/MRA. Ideally, the final contour of the treatment planning would encompass the AVM nidi or DAVFs depicted by 4D-DSA. From these 16 patients, it was observed that the isodose contour retrieved from the original treatment planning matched well with the nidi/fistulas viewed on 4D-DSA. In some cases, particularly with a large AVM nidus, 4D-DSA showed that the original treatment plan covered normal brain tissue. From statistical results, it was observed that the contoured AVMs, particularly large and intricate ones, of the 4D-DSA volumes were generally smaller than those contoured on integrated stereotactic imaging. Discrepancies between contoured DAVF volumes on 4D-DSA and integrated stereotactic imaging were larger and more frequently observed than that of AVMs. Such discrepancies may be attributed to beam-hardening artifacts resulting from the fistula itself or bones of the skull/skull base, as well as poor image contrast and the incorrect selection of optimal phases. An improved reconstruction algorithm and additional artifact reduction schemes may potentially reduce the impact of beam-hardening artifacts on 4D-DSA and facilitate 4D-DSA-based contouring for DAVF cases in the future.

Of particular interest is the patient with an AVM nidus that has multiple feeding arteries, as shown in the corresponding 4D-DSA volumes (Fig 6). The vertebral artery (Fig 6*A*) and right internal carotid artery (Fig 6*B*) jointly supply the AVM nidus (Fig 6*C*). Visually, 4D-DSA has better capability in differentiating the supplying territories of distinct feeding arteries than 2D-DSA projections. This feature suggests that the implementation of 4D-DSA and advanced imaging technology makes objective territorial separation of the AVM nidus, which is supplied by multiple arterial territories, more feasible. The ability to differentiate distinct arterial territories can be valuable for extremely large and intricate AVMs, where the nidus volume is considered too large to be safely treated by a single session of radiosurgery. In such cases, volume-staged radiosurgery that divides the radiosurgery into multiple sessions can be an effective alternative.[28] The treatment plan based on 4D-DSA will divide the AVM nidus into compartments that correspond to different feeding arteries; then a single session of radiosurgery will focus on a single compartment. The entire arterial territory of a single feeding artery will receive the full dose in a single radiosurgery session. Theoretically, this approach may yield a better treatment result because recanalization may have a greater chance to occur in incompletely treated compartments if the AVM nidus is not divided on the basis of arterial territories.

However, the study was limited by the small patient population; a larger patient population is warranted in subsequent studies. In addition, the tissue contrast of MR imaging, derived from

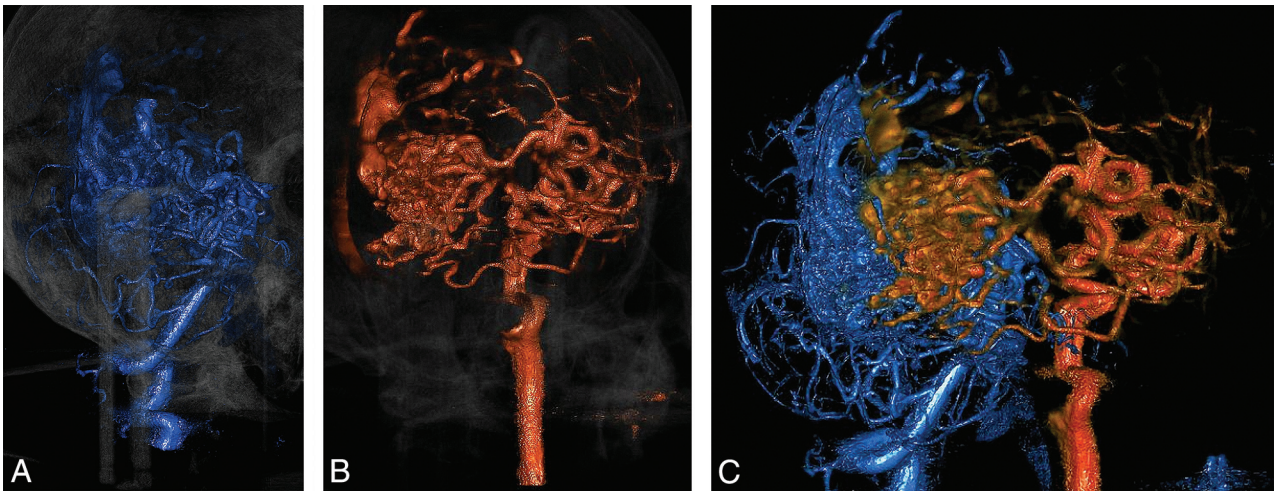

FIG 6. *A*, A 4D-DSA section of a 55-year-old man with a large AVM that is supplied by 2 arterial territories, viewed from the posterior left viewpoint. A portion of the nidus is revealed by left vertebral artery injection. *B*, Another 4D-DSA volume is viewed from the same direction as in *A*. The remaining portion of the nidus is revealed by right internal carotid artery injection. *C*, The whole AVM nidus is shown by fusing 2 distinct volumes (the left vertebral artery portion is blue, with the right internal carotid artery portion being orange). Objective separation between distinct arterial territories can be done by using 4D-DSA with selective administration of contrast medium. The 2 volumes may then be fused to provide a panoramic view of the AVM nidus.

large differences in T1 and T2 relaxation times among various tissues,[29] was superior to that of 2D-CT-like images. Also, because 4D-DSA involves an x-ray tube and flat panel detector rotation, the system resembles conebeam CT. Therefore, a certain degree of conebeam-related distortion may have contributed to registration errors encountered, though the distortion of conebeam CT generally lies within the submillimeter range.[30,31] Other x-ray-related artifacts may also hamper the ability of 4D-DSA to depict nidi/fistulas.[32] It was also observed that our current hardware is prone to misaligning due to a limited FOV, leading to incomplete coverage of the markers on the localization box, rendering the images unsuitable for registration during treatment planning.

Rudimentarily, 4D-DSA is a multiple phasic 3D-DSA. In the current study, 4D-DSA is equivalent to 304 phases of 3D-DSA. It is believed that 3D-DSA demonstrates AVM morphology better than MR imaging. 4D-DSA adds hemodynamics to 3D-DSA and its application value in AVM radiosurgery. The ability of 4D-DSA to demonstrate vascular morphology and hemodynamics in 4 dimensions potentially reduces the need and dependence of stereotactic MR imaging and shows its potential for 1-stop DSA in radiosurgery.[33]

Moreover, the 4D feature is not exclusive to a single manufacturer. Potentially, the 4D-DSA may be used in conjunction with conebeam CT angiography for both superior spatial resolution images and temporal information integrated into a single environment to achieve the best target delineation in radiosurgery.

CONCLUSIONS

Implementation of fully time-resolved 3D-DSA data into Gamma Knife radiosurgery for patients with brain AVM/DAVF is feasible. The AVM nidus volume contoured on 4D-DSA is generally smaller than that contoured on integrated stereotactic imaging because normal brain tissue is more easily distinguished. Also, objective territorial separation of the intricate AVM nidus, which is supplied by multiple arterial territories, may be easier to perform with 4D-DSA.

Disclosures: Chung-Jung Lin—*UNRELATED: Grants/Grants Pending:* Ministry of Science and Technology (grant number 104-2314-B-010-037).* Sonja Gehrisch—*UNRELATED: Employment*: Siemens. Markus Kowarschik—*UNRELATED: Employment*: Siemens. *Money paid to the institution.

REFERENCES

1. Steiner L, Greitz T, Leksell L. **Radiosurgery in intracranial arteriovenous malformation.** In: *Proceedings of the Sixth International Congress of Neurological Surgeons*, Amsterdam, the Netherlands. June 19–25, 1977
2. Steiner L, Leksell L, Forster DM, et al. **Stereotactic radiosurgery in intracranial arterio-venous malformations.** *Acta Neurochir (Wien)* 1974;(suppl 21):195–209 Medline
3. Steiner L, Leksell L, Greitz T, et al. **Stereotaxic radiosurgery for cerebral arteriovenous malformations: report of a case.** *Acta Chir Scand* 1972;138:459–64 Medline
4. Barcia-Salorio JL, Solis OJ, Barcia JA, et al. **Radiosurgery of carotid-cavernous fistulae.** *Acta Neurochir Suppl* 1994;62:10–12 CrossRef Medline
5. Wu HM, Pan DH, Chung WY, et al. **Gamma knife surgery for the management of intracranial dural arteriovenous fistulas.** *J Neurosurg* 2006;105(suppl):43–51 Medline
6. Friedman JA, Pollock BE, Nichols DA, et al. **Results of combined stereotactic radiosurgery and transarterial embolization for dural arteriovenous fistulas of the transverse and sigmoid sinuses.** *J Neurosurg* 2001;94:886–91 CrossRef Medline
7. Pan DH, Guo WY, Chung WY, et al. **Gamma knife radiosurgery as a single treatment modality for large cerebral arteriovenous malformations.** *J Neurosurg* 2000;93(suppl 3):113–19 Medline
8. O'Leary S, Hodgson TJ, Coley SC, et al. **Intracranial dural arteriovenous malformations: results of stereotactic radiosurgery in 17 patients.** *Clin Oncol (R Coll Radiol)* 2002;14:97–102 CrossRef Medline
9. Onizuka M, Mori K, Takahashi N, et al. **Gamma knife surgery for the treatment of spontaneous dural carotid-cavernous fistulas.** *Neurol Med Chir (Tokyo)* 2003;43:477–83 CrossRef Medline
10. Guo WY, Pan DH, Wu HM, et al. **Radiosurgery as a treatment alter-**

native for dural arteriovenous fistulas of the cavernous sinus. *AJNR Am J Neuroradiol* 1998;19:1081–87 Medline
11. Guo WY, Nordell B, Karlsson B, et al. **Target delineation in radiosurgery for cerebral arteriovenous malformation: assessment of the value of stereotaxic MR imaging and MR angiography.** *Acta Radiol* 1993;34:457–63 CrossRef Medline
12. Guo WY. **Radiological aspects of gamma knife radiosurgery for arteriovenous malformations and other non-tumoural disorders of the brain.** *Acta Radiol Suppl* 1993;388:1–34 Medline
13. Guo WY, Wikholm G, Karlsson B, et al. **Combined embolization and gamma knife radiosurgery for cerebral arteriovenous malformations.** *Acta Radiol* 1993;34:600–06 CrossRef Medline
14. Safain MG, Rahal JP, Raval A, et al. **Use of cone-beam computed tomography angiography in planning for gamma knife radiosurgery for arteriovenous malformations: a case series and early report.** *Neurosurgery* 2014;74:682–95; discussion 695–96 CrossRef Medline
15. Guo WY, Lindqvist M, Lindquist C, et al. **Stereotaxic angiography in gamma knife radiosurgery of intracranial arteriovenous malformations.** *AJNR Am J Neuroradiol* 1992;13:1107–14 Medline
16. Davis B, Royalty K, Kowarschik M, et al. **4D digital subtraction angiography: implementation and demonstration of feasibility.** *AJNR Am J Neuroradiol* 2013;34:1914–21 CrossRef Medline
17. Royalty K. *4D DSA: New Methods and Applications for 3D Time-Resolved Angiography for C-arm CT Interventional Imaging* [PhD dissertation]. Madison, Wisconsin: University of Wisconsin-Madison; 2014
18. Sandoval-Garcia C, Royalty K, Aagaard-Kienitz B, et al. **A comparison of 4D DSA with 2D and 3D DSA in the analysis of normal vascular structures in a canine model.** *AJNR Am J Neuroradiol* 2015;36:1959–63 CrossRef Medline
19. Sandoval-Garcia C, Royalty K, Yang P, et al. **4D DSA a new technique for arteriovenous malformation evaluation: a feasibility study.** *J Neurointerv Surg* 2016;8:300–04 CrossRef Medline
20. Lescher S, Gehrisch S, Klein S, et al. **Time-resolved 3D rotational angiography: display of detailed neurovascular anatomy in patients with intracranial vascular malformations.** *J Neurointerv Surg* 2016 Aug 4. [Epub ahead of print] CrossRef Medline
21. Conti A, Pontoriero A, Faragò G, et al. **Integration of three-dimensional rotational angiography in radiosurgical treatment planning of cerebral arteriovenous malformations.** *Int J Radiat Oncol Biol Phys* 2011;81:e29–37CrossRef Medline
22. Conti A, Pontoriero A, Iatì G, et al**. 3D-printing of arteriovenous malformations for radiosurgical treatment: pushing anatomy understanding to real boundaries.** *Cureus* 2016;8:e594 CrossRef Medline
23. Veeravagu A, Hansasuta A, Jiang B, et al. **Volumetric analysis of intracranial arteriovenous malformations contoured for CyberKnife radiosurgery with 3-dimensional rotational angiography vs computed tomography/magnetic resonance imaging.** *Neurosurgery* 2013;73:262–70 CrossRef Medline
24. Kang J, Huang J, Gailloud P, et al. **Planning evaluation of C-arm cone beam CT angiography for target delineation in stereotactic radiation surgery of brain arteriovenous malformations.** I*nt J Radiat Oncol Biol Phys* 2014; 90:430–37 CrossRef Medline
25. Söderman M, Guo WY, Karlsson B, et al. **Neurovascular radiosurgery.** *Interv Neuroradiol* 2006;12:189–202 Medline
26. Yu S, Yan L, Yao Y, et al. **Noncontrast dynamic MRA in intracranial arteriovenous malformation (AVM), comparison with time of flight (TOF) and digital subtraction angiography (DSA).** *Magn Reson Imaging* 2012;30:869–77 CrossRef Medline
27. Soize S, Bouquigny F, Kadziolka K, et al. **Value of 4D MR angiography at 3T compared with DSA for the follow-up of treated brain arteriovenous malformation.** *AJNR Am J Neuroradiol* 2014;35:1903–09 CrossRef Medline
28. Chung WY, Shiau CY, Wu HM, et al. **Staged radiosurgery for extra-large cerebral arteriovenous malformations: method, implementation, and results.** *J Neurosurg* 2008;109(suppl):65–72 CrossRef Medline
29. Mitchell DG, Burk DL Jr, Vinitski S, et al**. The biophysical basis of tissue contrast in extracranial MR imaging.** *AJR Am J Roentgenol* 1987;149:831–37 CrossRef Medline
30. Chang J, Yenice KM, Narayana A, et al. **Accuracy and feasibility of cone-beam computed tomography for stereotactic radiosurgery setup.** *Med Phys* 2007;34:2077–84 CrossRef Medline
31. Ruschin M, Komljenovic PT, Ansell S, et al. **Cone beam computed tomography image guidance system for a dedicated intracranial radiosurgery treatment unit.** *Int J Radiat Oncol Biol Phys* 2013;85:243–50 CrossRef Medline
32. Wowra B, Tonn J, Muacevic A. *Gamma Knife Radiosurgery European Standards and Perspective.* Vienna: Springer Vienna; 2004
33. Hung SC, Lin CJ, Guo WY, et al. **Toward the era of a one-stop imaging service using an angiography suite for neurovascular disorders.** *BioMed Res Int* 2013;2013:873614 CrossRef Medline